Conformationally selective photodissociation dynamics of propanal cation

Hongli Tao, Lei Shen, Myung Hwa Kim, Arthur G. Suits, and Todd J. Martinez

Citation: The Journal of Chemical Physics **134**, 054313 (2011); doi: 10.1063/1.3540659
View online: http://dx.doi.org/10.1063/1.3540659
View Table of Contents: http://scitation.aip.org/content/aip/journal/jcp/134/5?ver=pdfcov
Published by the AIP Publishing

Conformationally selective photodissociation dynamics of propanal cation

Hongli Tao,[1,2] Lei Shen,[3] Myung Hwa Kim,[4] Arthur G. Suits,[3] and Todd J. Martinez[1,2,a)]
[1]*PULSE Institute and Department of Chemistry, Stanford University, Stanford, California 94305, USA*
[2]*SLAC National Accelerator Laboratory, Menlo Park, California 94025, USA*
[3]*Department of Chemistry, Wayne State University, Detroit, Michigan 48202, USA*
[4]*Department of Chemistry and Nano Science, Ewha Womans University, Seoul 120-750, South Korea*

(Received 22 September 2010; accepted 21 December 2010; published online 4 February 2011)

We have previously reported experimental evidence for conformationally selective dissociation of propanal cation that was interpreted, on the basis of *ab initio* multiple spawning calculations, as arising from distinct dynamics in the excited state manifold of the cation. Two conical intersections (CIs) are accessible from Franck–Condon points on the dark state; however, different conformers prefer different CIs and quench to different regions on the ground state. In this paper, we extend our initial report to include experimental results for the partially deuterated propanal cation as well as detailed characterization of the ground state potential energy surface and statistical calculations of the ground state dissociation dynamics. The DC slice imaging experiments show a bimodal velocity distribution for H elimination with the observed branching ratio of the two channels different for the *cis* and *gauche* conformers. H(D)-elimination experiments from deuterated propanal cation support the dissociation mechanism proposed in the earlier report. We further investigate reaction rates on the ground state using Rice–Ramsperger–Kassel–Marcus theory. We find that the experimental results are consistent with a mechanistic picture where the ground state dissociation is statistical, and conformer specificity of the dissociation products arises because of the different populations in distinct ground state isomers after photoexcitation due to ultrafast quenching to the ground state. © *2011 American Institute of Physics*. [doi:10.1063/1.3540659]

I. INTRODUCTION

Conformational dynamics and conformational selectivity are crucial to chemical reactions and biological function. However, molecular conformers can often easily interconvert via rotations about a single bond and, thus, are difficult to study and control. Despite this limitation, there have been several experimental and theoretical studies on conformation-specific chemistry, including *cis*-, *trans*-formic acid photodissociation in an argon matrix,[1] direct *gauche*-, anti-l-iodopropane photodissociation from a repulsive excited state,[2] photodissociation of axial and equatorial conformers of morpholine,[3] and a theoretical study of photoionization of different glycine conformers.[4] We recently reported a study of the photodissociation dynamics of *cis* and *gauche* propanal cation,[5] wherein a specific conformer cation was prepared by resonance-enhanced multiphoton ionization REMPI (Refs. 6 and 7) and further electronically excited by another photon. The velocity distribution for the H elimination product was bimodal for both conformers; however, the branching ratio between the two components was found to be strongly conformer dependent. To understand the mechanism, the *ab initio* multiple spawning (AIMS) method[8] was used to study the excited state dynamics of both conformers. Distinct dynamics were seen for trajectories initiated from the Franck–Condon (FC) regions of the two starting conformers, as discussed in greater detail below. However, the absence of anisotropy of the experimental ion images suggests that dissociation ultimately takes place on the ground electronic state in statistical fashion. This makes the observed conformer specificity even more surprising—somehow the dissociation retains memory of the starting conformer and simultaneously exhibits signatures of statistical energy redistribution. This is so even though the energetic difference between conformers is only $\approx 400\,\mathrm{cm}^{-1}$ which is negligible compared to the $\approx 30\,000\,\mathrm{cm}^{-1}$ imparted by photon absorption. In this work, we investigate the ground state energetics and decomposition kinetics of $C_3H_6O^+$ using traditional Rice–Ramsperger–Kassel–Marcus (RRKM) theory[9,10] to complete our understanding of the conformationally mediated dynamics seen in the experiment. We show that the conformer selectivity is imposed very early in the dynamics through a conformer-specific distribution of population that returns to the D_0 ground state, and that memory of this conformer-specific distribution persists even though the ground state dissociation dynamics spans the picosecond to nanosecond time scale.

As the simplest radical cation with the CCCO frame, the $C_3H_6O^+$ radical cation has been studied extensively both experimentally[11–14] and theoretically.[15–17] Our work here also provides further understanding of the isomerization and decomposition processes in this molecule, although we focus primarily on understanding the conformer selectivity. The rest of this article is organized as follows: Sec. II reports the experiment, including a brief description of the previous normal propanal cation photodissociation study as well as results for the new partially deuterated cases. The simulation methods used to study the system are described in Sec. III. In Sec. IV, both the experimental and theoretical results are

a)Author to whom correspondence should be addressed. Electronic mail: todd.martinez@stanford.edu.

discussed and compared to each other. And finally, this work is summarized in Sec. V.

II. EXPERIMENT

The detailed description of our apparatus has been presented elsewhere.[18] Propanal is kept in a glass bubbler at room temperature, with He carrier gas at a backing pressure of ~3 atm. The gas mixture is introduced through a piezoelectric pulsed nozzle with a l mm orifice into the source chamber of our differentially pumped apparatus. After passing through the skimmer located 3.8 cm downstream of the pulsed valve, the supersonic molecular beam enters into the velocity mapping ion optics assembly consisting of four electrodes. The molecular beam is perpendicularly intersected with a laser beam tuned to a two-photon resonant excitation of the (n, 3 s) Rydberg state of propanal. The operating pressures are maintained at $\sim 3.0 \times 10^{-6}$ Torr in the source chamber and less than 5×10^{-8} Torr in the main chamber.

The laser beam is generated by frequency doubling the output of a dye laser (Scanmate, LDS 698, LDS 722) pumped by the second harmonic of an Nd : YAG laser (Spectra-physics, GCR-5). The laser is focused with a lens ($f = 30$ cm) into the interaction volume. Typical output power of the laser beam is 1–2 mJ/pulse and wavelength calibration is achieved by a wavemeter (Coherent WaveMaster). Following ionization and dissociation, the product ions are accelerated through a multilens velocity mapping assembly, with the voltage settings typically : 1000, 800, 300, and 0 V. After passing through a field-free region, the particles impact upon a position sensitive dual MCP/P-47 phosphor screen of 120 mm diameter (Burle/Photonis) located 150 cm downstream from the interaction region. The resulting images are recorded by a CCD camera (Sony, XC-ST50) implemented with the IMACQ megapixel software,[19] developed in our group, which permits real-time event counting and centroiding of the data. These images are integrated over ~200 000 laser shots.

Normal propanal (99%, Aldrich) is used without further purification. Partially deuterated propanal ($CH_3CD_2CHO/CH_3CHDCHO$) mixture was synthesized via the direct deuterium exchange reaction with an equal amount of D_2O (99.98%, Aldrich) and 5% v/vN, N-dimethyl-l, 3-propanediamine (97%, Aldrich) from n-propanal in the following scheme:

$$CH_3CH_2CHO \xrightarrow[RT/2hrs]{D_2O/CH_3NHCH_2CH_2CH_2NHCH_3} CH_3CHDCHO + CH_3CD_2CHO.$$

After finishing the reaction, the organic layer containing the deuterated propanal mixture was separated and used without further purification. The isotopologue of interest could largely be selected spectroscopically, so that contamination of the sample by other species did not greatly interfere with the experiment. For H loss from CH_3CD_2CHO, there was no interference from $CH_3CHDCHO$, as it could not give a contribution at mass 59. For D loss from CH_3CD_2CHO, some interference from H loss from $CH_3CHDCHO$ (both mass 58) was seen for the *gauche* species, as spectroscopic selection was not complete on that transition.

III. THEORY

We use the *ab initio* multiple spawning (AIMS) method[8] to investigate the excited state dynamics for both *cis* and *gauche* propanal cations.[5] The AIMS method solves the electronic and nuclear Schrödinger equations simultaneously and allows for the seamless treatment of dynamics on multiple electronic states and bond rearrangement. The total wavefunction in AIMS is written as

$$\Psi(r, R, t) = \sum_I \chi_I(R, t)\phi_I(r; R), \quad (1)$$

where the index I denotes the electronic state, $\phi_I(r; R)$ is the electronic wavefunction of state I and $\chi_I(R, t)$ is the time-dependent nuclear wavefunction associated with the Ith electronic state. Each of the nuclear wavefunctions χ_I is itself expanded as a linear combination of travelling frozen Gaussian basis functions[20,21] (trajectory basis functions or TBFs). Each of the TBFs evolves according to classical equations of motion with an additional semiclassical phase factor.[8] The initial conditions for each TBF are determined by sampling from the Wigner distribution corresponding to the ground vibrational state in the harmonic approximation. In order to describe nonadiabatic events, e.g., at or near conical intersections, the basis set of TBFs is expanded adaptively through a spawning procedure. Specifically, a new basis function is created when an existing basis function enters the region where two or more electronic states are strongly coupled. Details of the spawning procedure may be found in past articles.[8,22,23] The widths of the TBFs do not evolve in time and are chosen according to a standard procedure.[24] The electronic structure, including the nonadiabatic coupling matrix elements between electronic states, is obtained on-the-fly, i.e., simultaneously with the solution of the dynamical equations. This allows the flexible description of different kinds of potential energy surfaces (PES) and chemical processes, including isomerization and bond rearrangement. Since the photodissociation of propanal cations involves multiple electronic states, we choose the complete active space SCF (CASSCF) method to calculate the electronic structure.[25–27] Specifically, the AIMS simulations are carried out with the SA3-CAS(5/5)/6-31G** method, which includes five electrons in a five orbital active space, averaging (with equal

weights) over the lowest three doublet states. As is well known, the CASSCF method does not provide a good description of dynamic electron correlation effects. Thus, we validate important aspects of the PES obtained from CASSCF by direct comparison to results obtained with both single-state[28] and multistate[29] multireference perturbation theory (CASPT2 and MS-CASPT2, respectively). All electronic structure calculations were performed using MOLPRO,[30] and AIMS simulations were carried out with FMS-MOLPRO.[31]

The AIMS method is well suited to the description of nonadiabatic dynamics occurring after photoexcitation. However, subsequent dynamics on the ground state may require long time scales when the reactions of interest are activated. This is the case for the present experiment, where the propanal cation dissociates on the ground state on the nanosecond (or longer) time scale. In fact, it is the first dissociation products (after H atom loss) that are measured in the experiment. Thus, we augment the short time AIMS dynamics with the RRKM treatment to describe the longer time dissociation. There are three ground state products formed within the first 100 fs after photoexcitation: *cis*- and *gauche*-propanal cation ($CH_3CH_2CHO^+$) and a H-migration product ($CH_3CHCH_2O^+$), as discussed below. We use the results of AIMS dynamics to determine the initial populations of these products on the ground state, which depend on which conformer (*cis* or *gauche*) was excited. The ultimate fate of the ground state products is then determined using the RRKM treatment and kinetic modeling, i.e., we assume that all subsequent reactivity after quenching from the excited state manifold is statistical. As discussed previously,[5] the isotropy of the ion images observed in the experiment supports this assumption.

Energetics (and optimized geometries and reaction paths) for the RRKM treatment were obtained using CAS(5/5)-PT2/6-31G**, which includes dynamic electron correlation effects. Transition states were located using the climbing image nudged elastic band (CINEB) algorithm introduced by Henkelman *et al.*[32] In order to simplify the computation, we first located all transition states between paths connecting all pairs of ground state minima using CINEB with a lower level of electronic structure, CAS(5/5)/6-31G**. Transition states corresponding to reaction barriers less than 3.5 eV (the available experimental energy after photoexcitation is 3.4 eV, relative to the *cis* propanal cation) were retained and refined using the more costly CASPT2 electronic structure method. Reaction rates were calculated using the CASPT2 energetics and RRKM theory with the Beyer–Swinehart direct state counting method.[9,10] Zero-point energy (ZPE) corrections were computed using CASPT2 frequencies. These reaction rates were, then, used to construct a kinetic model that was solved in order to determine the branching ratio of products starting from the initial distribution of short-time ground state products predicted by AIMS. In addition, in order to understand the follow-up deuterated experiment, we also investigated the excited state dynamics and the ground state reactions for the partially and fully deuterated propanal cation.

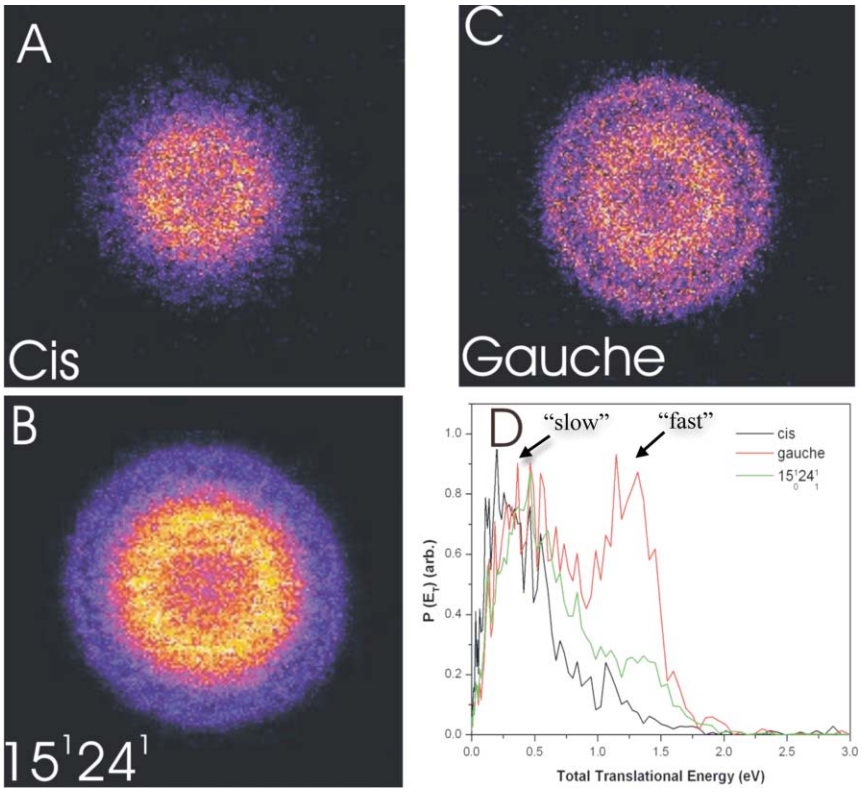

FIG. 1. (a–c) Sliced ion images of the $C_3H_5O^+$ product of propanal cation photodissociation, starting from the *cis* (a and b) or *gauche* (c) conformer. In panels (a) and (c), the cation is prepared in the vibrational ground state, while in (b) the *cis* conformer is prepared in a well-defined vibrational excited state. (d) Total translational energy distributions from the images in (a–c). $P(E_T)$ is the probability of a given translational energy (E_T) (arbitrary units).

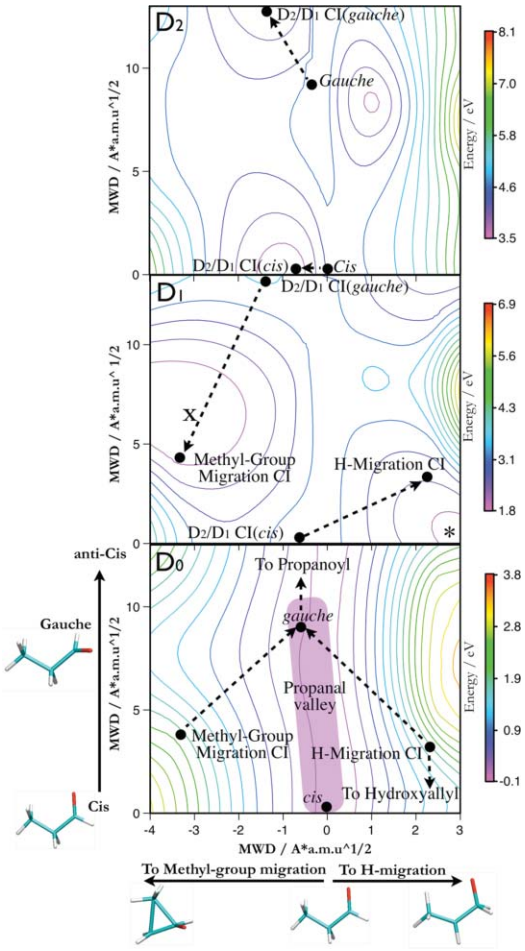

FIG. 2. Contour plot of interpolated PES and pathways on these surfaces, computed with SA-3-CAS(5/5) and the $6-31G^{**}$ basis set. Along the x axis are mass-weighted distance from propanal (*cis*) to methyl-group migration geometry (negative) and to H-migration geometry (positive). Y axis is mass-weighted distance from *cis* to *anticis* propanal, passing through the *gauche* conformer. Important points on the PES are labeled with black dots.Upper: D_2 (bright state). *Cis* and *gauche* conformers quickly quench to D_1 through nearby conical intersections (distinct for each conformer). Middle: D_1 (dark state). The *gauche* conformer relaxes to a CH_3-migration minimum (denoted as x), quenching to D_0 near the indicated D_1/D_0 intersection with CH_3-migration character. The *cis* conformer relaxes to the H-migration minimum (denoted as $*$), quenching to D_0 near a D_1/D_0 intersection with H-migration character. Lower: D_0 (ground state). Population that quenches through the CH_3 migration D_1/D_0 intersection (originating from the *gauche* conformer) promptly returns to the propanal geometry and dissociates to propanoyl cation (the faster channel in Fig. 1). Population that quenches through the H migration D_1/D_0 intersection (originating from the *cis* conformer) is split between return to the propanal geometry and prompt elimination of a H atom to form hydroxyallyl cation (the slower channel in Fig. 1).

IV. RESULTS AND DISCUSSION

The preliminary experimental results have been reported before for the nondeuterated propanal cation:[5] the conformationally selected propanal cation is generated through a $2+1$ REMPI process in a well-defined vibrational level, characterized in detail previously.[33] Absorption of a fourth photon induces photodissociation of the cation and the $C_3H_5O^+$ product (after H or D atom elimination) is monitored by ion imaging. The $C_3H_5O^+$ product can further decompose (secondary decomposition), losing either CO or CHO^+.

Three images of product $C_3H_5O^+$ are shown in Fig. 1, along with the total translational energy distributions.

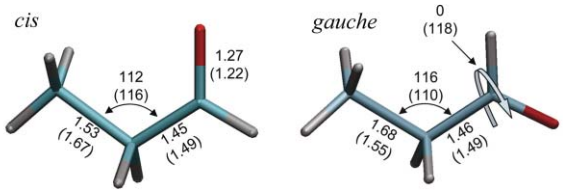

FIG. 3. D_2/D_1 minimal energy conical intersection (MECI) geometries for *cis* (left) and *gauche* (right) propanal cation as optimized with SA-3-CAS(5/5) and the $6-31G^{**}$ basis set. Selected bond lengths (Angstroms) and angles (degrees) are shown for the MECI geometry and for the Franck–Condon geometry (in parentheses). The MECI accessed by the *cis* form is only slightly different from the FC point. The MECI accessed by the *gauche* form differs from the FC point primarily in the labeled dihedral angle, which is *gauche* at the FC point and *trans* at the D_2/D_1MECI accessed by the dynamics.

Images were acquired for dissociation of vibrationless *cis* (539 43.9 cm^{-1}) and *gauche* (547 85.3 cm^{-1}) propanal cation and for the *cis* ion with one quantum of v_{15} (CCCO backbone deformation)$-v_{24}$ (CHO torsion) combination mode excitation (541 72.1 cm^{-1}). All the images show two rings, indicating there are two distinct product channels. However, the intensity of the outer ring varies according to the initial conformer of propanal cation and the initial vibrational level. The translational energy distributions derived from the images, thus, show two peaks for each transition with different relative intensities; the fast peak is assigned as propanoyl cation ($CH_3CH_2CO^+$) and the slow peak as hydroxyallyl cation ($CH_2CHCHOH^+$) on the basis of translational energy release and secondary decomposition thresholds. The relative yield of the fast component varies with vibrational level and conformational isomer: 16% for the *cis* conformer, 24% for the $15_0^1 24_1^1$ vibrationally excited *cis* conformer, and 44% for the *gauche* conformer. Unfortunately, the observed relative yields do not correspond to the branching ratio of the initial H elimination reactions because they do not account for the efficiency of the secondary decomposition process, which will be different for the propanoyl and hydroxyallyl cations. Thus, although we could predict the product branching ratios, these would not be directly comparable to the data obtained in this experiment. Nevertheless, the difference in the observed relative yields provides clear evidence of a conformational specificity in the excited state dynamics.

To investigate the origin of the branching ratio difference observed in the experiment, we first performed excited state dynamics for both conformers (nondeuterated and starting in the vibrational ground state) using AIMS. The dynamics simulations start from the second excited state (D_2), which corresponds to an optically bright $\sigma \rightarrow n$ transition. The lower lying first excited state (D_1) is optically dark and corresponds to a $\pi \rightarrow n$ transition centered on the carbonyl group. Five initial conditions were sampled for each of the *cis* and *gauche* starting conformers. The AIMS simulations showed significant (up to 50%) rapid and efficient transfer from the bright D_2 state to the lower lying dark D_1 state within approximately 10 fs, before any appreciable motion of the nuclei is possible.[5] This is because the Franck–Condon point is very close to a D_2/D_1 conical intersection in both conformers, as indicated in Fig. 2. However, the D_2/D_1 intersection that is accessed is *different* for each of the *cis* and *gauche* conformers. Thus,

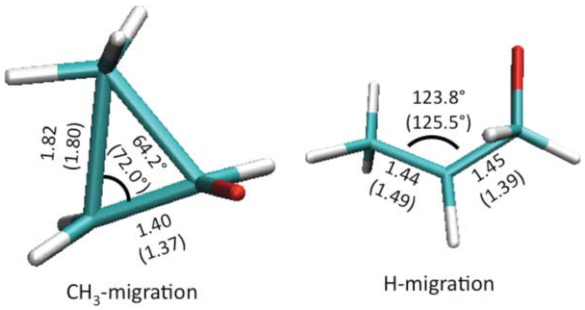

FIG. 4. Distinct minima on D_1 optimized with SA-2-CAS(5/5)-MSPT2/6-31G**. *Gauche* or *cis* conformers of propanal cation excited to the bright D_2 excited state relax primarily to the CH_3-migration D_1 minimum (left) or the H-migration D_1 minimum (right), respectively. Selected geometric parameters (Angstroms and degrees) are shown, with results from SA-3-CAS(5/5)/6-31G** optimization in parentheses. Optimized minimal energy D_1/D_0 conical intersections are within 3 kcal/mol of these minima at both the CAS and MSPT2 levels. Since the geometries of these MECIs are very close to the displayed D_1 minima, they are not shown.

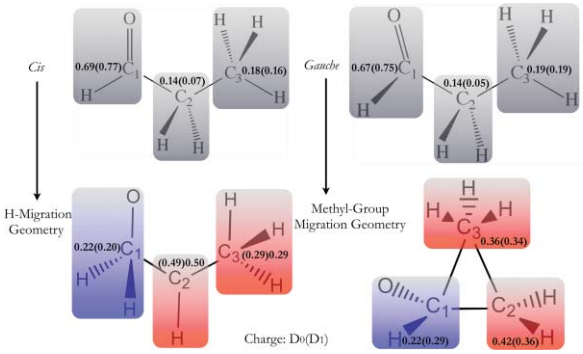

FIG. 5. Mulliken charge analysis of CASSCF wavefunctions at D_0 and D_1 minima (upper and lower panels, respectively). Charges for D_1 are shown in parenthesis and grouping of atoms for the charge analysis is shown with shaded boxes. The positive charge of both *cis* and *gauche* propanal cation (upper left and upper right, respectively) in the ground state is largely localized on the carbonyl group. At both of the D_1 minima (H-migration, left and CH_3-migration, right),the charge on the carbonyl group decreases (indicated by blue shading) and the charge on the remaining groups increases (indicated by red shading).

the *cis* and *gauche* conformers arrive on the dark D_1 state in different geometries (very close to the corresponding starting geometry). The minimal energy D_2/D_1 conical intersections (optimized at the CASSCF level used in the dynamics) are shown in Fig. 3, along with selected geometric parameters compared to the respective Franck–Condon point.

There are two minima on D_1 corresponding to H-migration and CH_3-migration, as indicated in Fig. 2 (denoted as $*$ and x, respectively). Detailed geometric parameters from optimization at the CAS and MS-CASPT2 levels are given in Fig. 4. We have argued previously that these distinct minima can be rationalized on the basis of the localization of the charge in the excited state. There are three likely possibilities for the location of the positive charge, if it were quasilocalized[34] – the terminal CHO, the central CH_2, or the terminal CH_3 groups. The stable *cis* and *gauche* D_0 minima correspond to localization of the positive charge on the terminal CHO group, as shown in Fig. 5. This is expected to be (and is) the most stable arrangement since it corresponds to removing an electron from the nonbonding O orbital of propanal. If the positive charge were instead localized on the methyl group, the molecule could be described as $CH_2=CHO$ in close proximity to CH_3^+. A strong cation $-\pi$ interaction is then expected, and the most favorable geometry should have the CH_3^+ bridging the C = C double bond.[35] This is exactly the geometry of the CH_3 migration D_1 minimum. As expected from the electrostatic nature of the cation $-\pi$ interaction, there is considerable delocalization of the π electrons onto the CH_3^+ moiety. Thus, the positive charge on the CH_3 moiety is lowered from its ideal value in the Mulliken analysis shown in Fig. 5.[36] Finally, the positive charge could be localized on the central CH_2 group and this would be stabilized by migration of a H atom to the CHO group. This is the geometry of the H-migration minimum on D_1, and Fig. 5 shows that much of the positive charge resides on the central CH group.

Because of the fast decay from D_2 to D_1 so close to the Franck–Condon point, it can be expected that there will be little qualitative difference between excitation to D_2 or D_1. Thus, we carried out AIMS dynamics exciting to D_1 (a further five initial conditions for each conformer). The resulting population dynamics are shown in Fig. 6. Almost half of the population has returned to D_0 within the simulation window

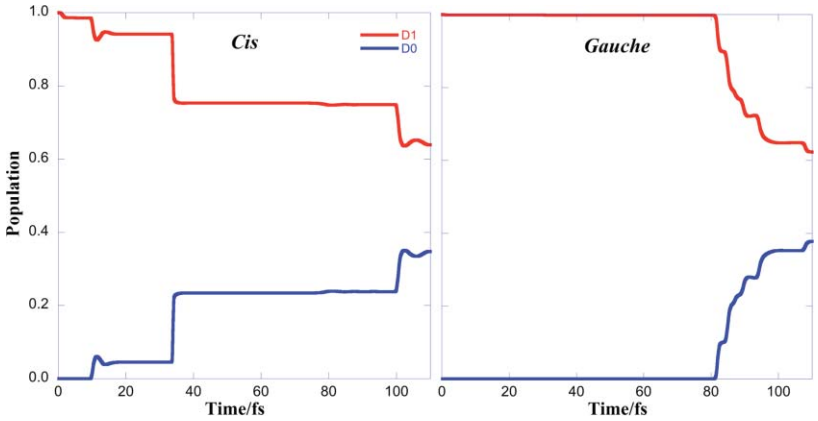

FIG. 6. Population dynamics for AIMS simulations of propanal cation after excitation to D_1. Almost half of the population returns to the ground state within 120 fs.

of 120 fs. On average, each simulation spawns two further trajectory basis functions during the simulation. Interestingly, the product on D_0 depends sensitively on the D_1/D_0 intersection that is accessed and this leads to a significant change in the character of the population on D_0 according to starting conformer. Starting with the *cis* conformer, 43% of the quenched population is in a H-migration-like geometry, i.e., CH_3CHCH_2O, and the remainder is in a propanal-like geometry (both *cis* and *gauche* conformers). In contrast, for the simulations that start with the *gauche* conformer, all quenched population is in a propanal-like geometry. The remaining population on D_1 at the end of the simulations is well characterized according to one of the two D_1 minima and is expected to quench to D_0 through the corresponding D_1/D_0 intersection. Analysis of the simulation data shows that 32%/73% of the D_1 population is trapped in the H-migration minimum for simulations starting with the *gauche*/*cis* conformers, respectively. Thus, we predict that starting with the *cis* conformer leads to 60% of the population trapped in the H-migration geometry on D_0 (the remainder being characterized as propanal). In contrast, starting with the *gauche* conformer leads to only 20% of the population in the H-migration minimum on D_0. A more quantitative estimate would require more initial conditions and longer simulations, but these results clearly show that the distribution of products on D_0 after excitation depends on the initially excited conformer. The origin of this discrimination can be seen in Fig. 7, where we show linear interpolation paths connecting the Franck–Condon point and either of the distinct D_1 minima, for each of the *cis* and *gauche* conformers. Starting from the *cis* conformer, the molecule arrives on D_1 and finds itself on a steep slope leading toward the H-migration minimum. In contrast, starting from the *gauche* conformer, the molecule arrives on a steep slope leading toward the CH_3-migration D_1 minimum. Figure 7 also compares the D_1 and D_0 potential energy surfaces from CASSCF and CASPT2 electronic

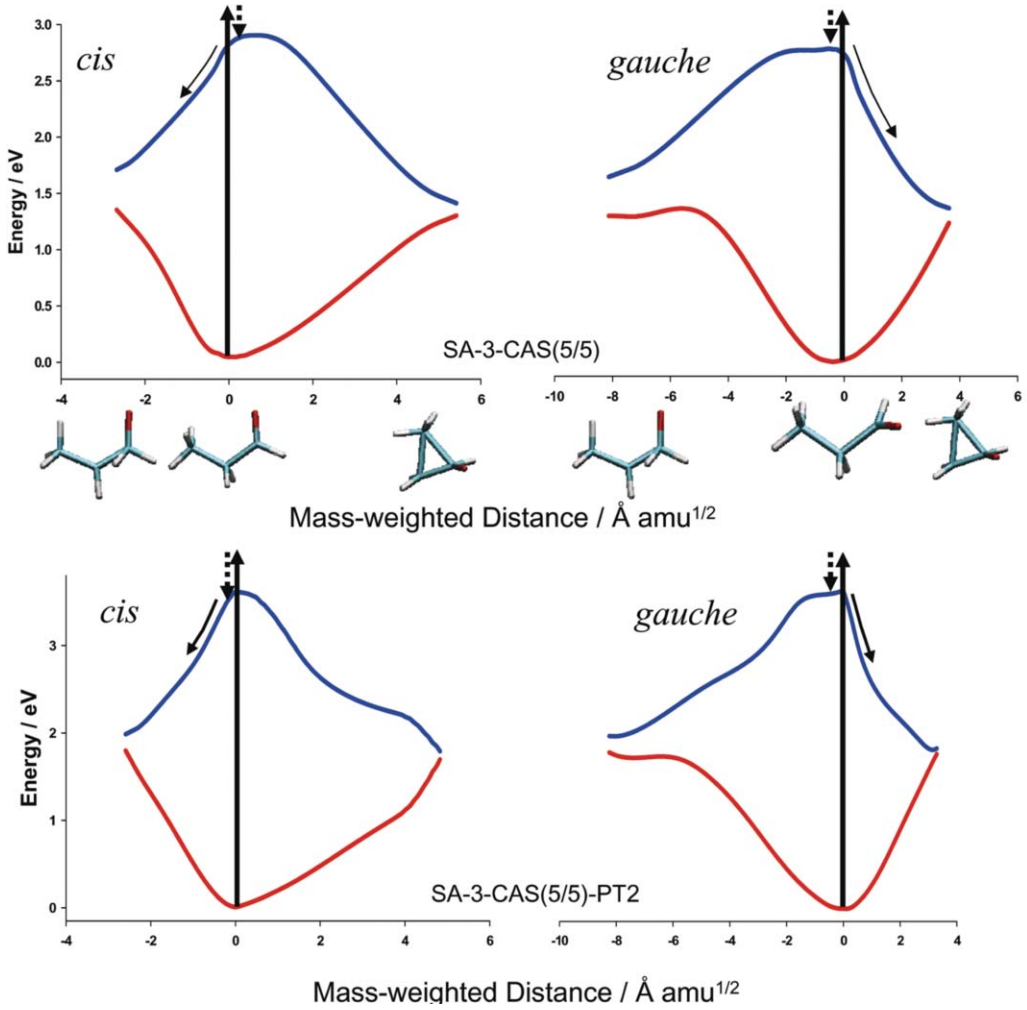

FIG. 7. Linear interpolation (in internal coordinates) from the FC point to each of the D_1 minima for *cis* (left) and *gauche* (right) forms of propanal cation. The upper two panels are obtained using the SA-3-CAS(5/5) method with a 6-31G** basis set, which is the electronic structure method used in the AIMS dynamics simulations. The solid vertical arrow represents the initial photoexcitation to D_2, and the dashed vertical arrow represents the fast internal conversion from D_2 to D_1. The lower two panels are obtained using the SA-3-CAS(5/5)-PT2 method with a 6-31G** basis set. This latter method includes dynamic electron correlation effects and it is in qualitative agreement with the CASSCF results. In all cases, the x axis is given in mass-weighted distance, so that the slope of the curves is an accurate representation of the relevant forces including kinematic effects. The qualitative features which lead to distinct products for the two conformers, namely the large difference in slopes toward different products in the FC region, are preserved in both electronic structure methods and emphasized here with diagonal arrows indicating the direction which dominates in each case.

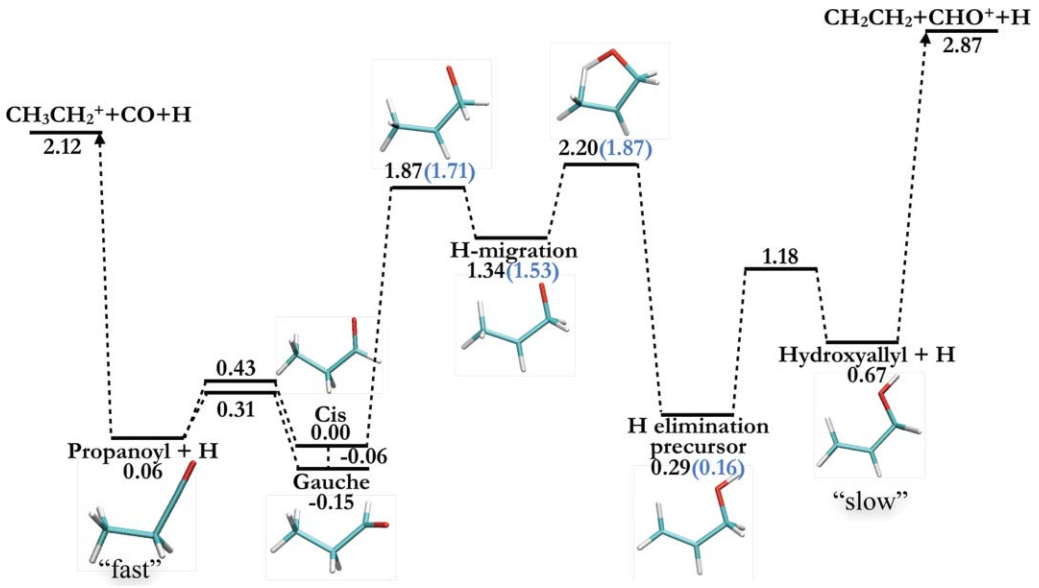

FIG. 8. Schematic pathways for H elimination reactions on the ground state surface. CASSCF energies are shown in black and selected MS-CASPT2 values (from full optimization of reactants, products and transition states using MS-CASPT2) are shown in blue. Geometries for the minima and selected transition states are shown.

structure theory, showing that the same picture holds even when dynamic electron correlation effects are included.

The remaining question is whether the nascent product distribution on D_0 makes any difference to the final products. After all, the molecule now has ≈3.4 eV of energy imparted to it from the photon, enough to surmount a number of isomerization barriers on the ground state. In order to fully understand the influence of the nascent D_0 product distribution on the final fragmentation, we have characterized minima on D_0 and barriers connecting these minima. As mentioned above, we located D_0 minima (a total of 16, including conformers) and transition states using CASSCF, taking into account minima located in previous theoretical studies.[16,17,37] All minima were then optimized with CASPT2 along with transition states corresponding to barriers of less than 3.5 eV at the CASSCF level. The full set of D_0 minima (geometries and energies) and transition states connecting them are detailed in Table Sl of the supporting information.[38] A summary of the most important geometries and energetics is shown in Fig. 8. The two most likely hydrogen-loss channels lead to propanoyl and hydroxyallyl cations, which both have $C_3H_5O^+$ stoichiometry and, thus, will be imaged by the experiment. These are expected to fragment almost exclusively as

$$\text{propanoyl } (CH_3CH_2CO^+) \Rightarrow CH_3CH_2^+ + CO,$$
$$\text{hydroxyallyl } (CH_2CH_2CHO^+) \Rightarrow CH_2CH_2 + CHO^+.$$

These secondary decomposition processes can occur on the time scale of the experiment and will deplete some of the $C_3H_5O^+$ product that would otherwise be imaged. Since the degree of secondary decomposition for each of the propanal/hydroxyallyl species during the time scale of the experiment is unknown, the precise branching between the two products cannot be inferred from the ion images in Fig. 1. The most important point to notice in Fig. 8 is that the H-migration minimum on D_0 can escape either to reform propanal (to the left in Fig. 8) or to form a "H-elimination precursor" (to the right in Fig. 8). If the molecule forms the H-elimination precursor, hydrogen atom dissociation (to form hydroxyallyl) is 3 orders of magnitude faster than isomerization back to the H-migration minimum (Table S2 in supporting information). Similarly, if the molecule escapes from the H-migration minimum to form propanal, hydrogen atom dissociation (to form propanoyl) is much faster than isomeriza-

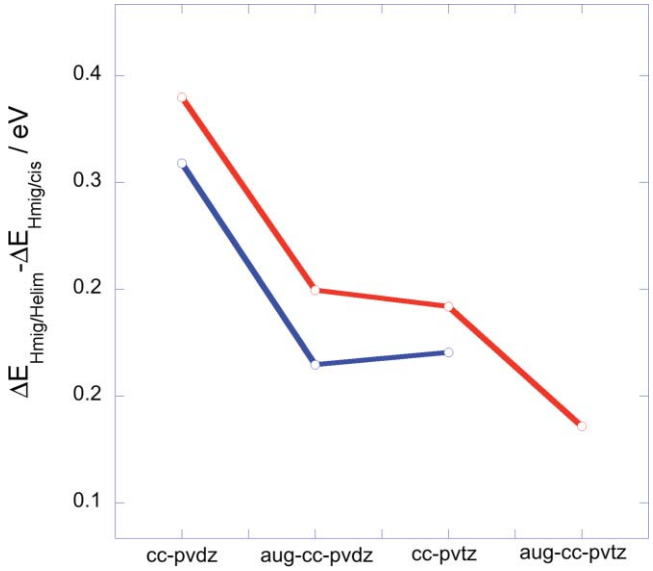

FIG. 9. Sensitivity to basis set and active space of the difference between two key barrier heights for escape from the H-migration D_0 minimum. See Fig. 8 for the relevant geometries. The barrier heights for these two reactions H − migration ⇒ *cis*-propanal and H − migration ⇒ H−elimination-precursor were computed (including complete reoptimization of the reaction path at each level of theory) using CAS(5/5)-PT2 (red line) and CAS(7/7)-PT2 (blue line) for a series of increasingly accurate basis sets. The ordering of the barrier heights is invariant, and the barriers become closer as the basis set is increased. ZPE corrections are included in the reported barrier heights, using harmonic frequencies computed at the indicated level of theory.

tion back to the H-migration minimum. Therefore, the two barriers (or more generally the associated rates) for escape from the H-migration minimum are critical in determining the final product distribution. Thus, we have investigated the dependence of these barrier heights on the electronic structure method, specifically active space and basis set. The difference between the two key barrier heights is shown in Fig. 9, where we extend the basis set up to augmented triple zeta and both (5/5) and (7/7) active spaces are used. In these calculations, all quantities (reactant and product geometries, transition states, and frequencies) are recalculated and optimized at the given level of theory. Extending the active space has little influence on the difference between these two barrier heights. The two barrier heights get closer as the basis set increases, which will increase the conformational selectivity, *vide infra*. Detailed energetics used to compute the difference between these barriers can be found in Fig. S4 of the supporting information.[38]

We carried out microcanonical RRKM analysis using the Beyer–Swinehart method, with energetics and frequencies obtained at the CASPT2 level of theory. For all reactions, energetics and frequencies from the CAS(5/5)-PT2/6-31G** method are used. The resulting reaction rates (a total of 60 reactions) at the experimental energy of 3.4 eV are given in Tables S2 and S3 of the supporting information.[38] These rates were then used in a kinetic model, starting with all population in one of the *cis*-propanal, *gauche*-propanal or H-migration minima. The experimental conditions are essentially collisionless for the time of interest and, therefore, we do not allow for collisional energy transfer in the kinetic model. More sophisticated models including collisional energy transfer could be considered in the future, for example using the multiwell program.[39] The results from kinetic modeling are shown in Fig. 10, where it can be seen that *cis*-propanal decays exclusively to the propanoyl product. In contrast, population that begins in the H-migration minimum decays to a mixture of hydroxyallyl and propanoyl products. The detailed branching ratios are given in Table I. We can conclude that the nascent product distribution on D_0 does have a significant influence on the final products, primarily because the H-migration minimum on D_0 is the only viable source of hydroxyallyl (both *cis* and *gauche* propanal conformers form propanoyl almost exclusively). One can compute the predicted fraction of hydroxyallyl product (the slow channel in Fig. 1) for excitation of the *cis*/*gauche* conformers from the dynamics and RRKM data. We emphasize that this is a rough estimate given the limited statistics for the dynamics and furthermore, the result could be quite sensitive to the precise values of the barrier heights for rearrangements of the H-migration minimum geometry. With these caveats, the result is 13%/4% production of hydroxyallyl (slow channel) for excitation of the *cis*/*gauche* conformer, respectively. This is a large influence, but the difference appears even more dramatic in the experiment because much of the propanoyl cation is lost to secondary dissociation; and the ion images are, thus, more sensitive to the minor hydroxyallyl product than might otherwise have been expected.

TABLE I. Branching ratios between propanoyl cation (fast channel) and hydroxyallyl cation (slow channel) starting from the three structures populated on D_0 after photoexcitation. Starting from either of the *cis* or *gauche* conformers of propanal cation leads almost exclusively to propanoylcation. In contrast, starting from the H-migration geometry leads to a mixture of propanoyl and hydroxyallyl cations. These results are obtained from RRKM modeling of rates at the experimental energy of 3.4 eV as described in the text.

Initial condition	Propanoyl cation (%)	Hydroxyallyl cation (%)
cis-propanal	97.5	1.1
gauche-propanal	99.6	0.2
H-migration	78.0	22.0

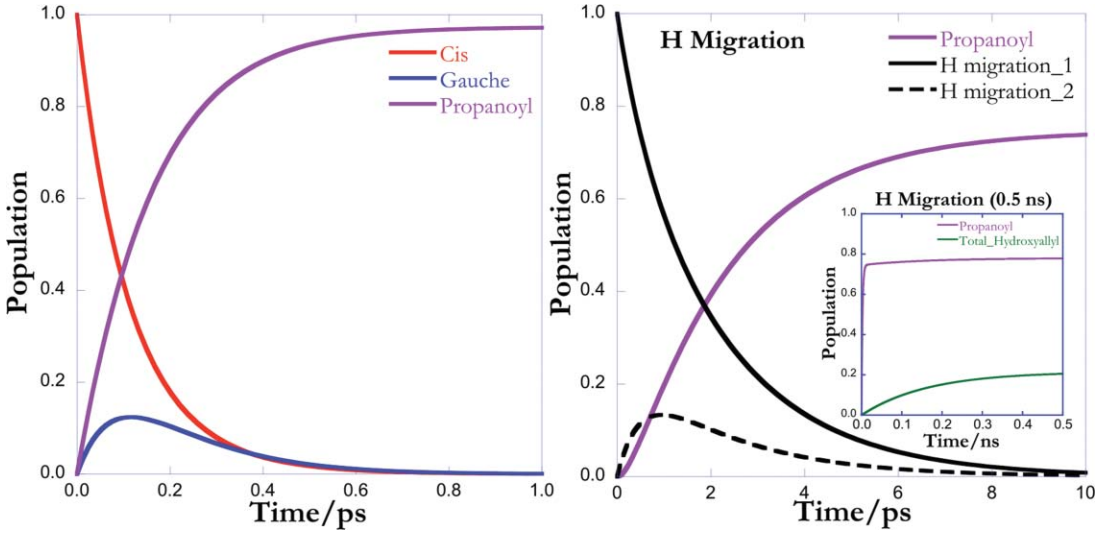

FIG. 10. Solution of rate equations based on RRKM rates starting from *cis* propanal (left) or the H migration product (right). Note the different time scales. When starting from *cis*-propanal (left), almost all of the population dissociates to propanoyl cation (fast channel) within 1 ps. When starting from the H-migration product (right), 78% dissociates promptly (within 10 ps) topropanoyl and the remainder dissociates to hydroxyallyl on the nanosecond time scale.

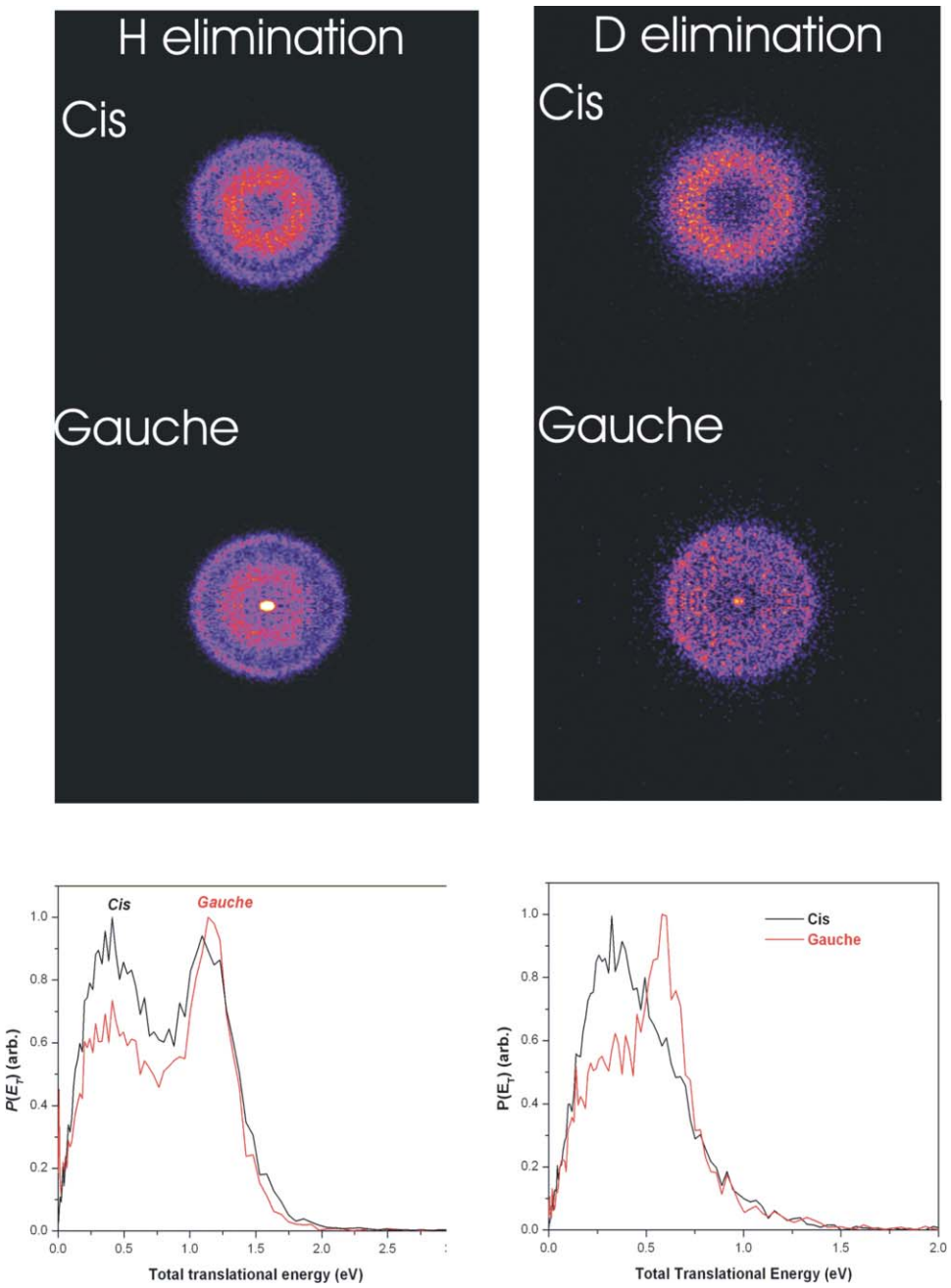

FIG. 11. The left panels are sliced ion images of the H elimination channel and respective total translational distributions of *cis* and *gauche* deuterated propanal. The right panels are sliced ion images of the D elimination channel and the respective total translational distributions of the two conformers.

In order to further investigate the detailed hydrogen elimination dynamics in this photodissociation event, partially deuterated propanal was used in follow-up experiments. The images of H atom and D atom elimination products from dissociation of are shown in Fig. 11. For the H elimination images, there are always two rings. However, the results are in sharp contrast with the normal propanal: the outer ring of the *cis* conformer is almost as intense as the inner ring and the inner ring of the *gauche* conformer is not as strong as the outer ring. This difference is more clearly shown in the total translational energy distribution diagram in Fig. 11. The intensity of the two peaks is almost the same for the *cis* conformer; while for the *gauche* conformer, the slow component reduces to almost half of normal (undeuterated) propanal. Here we should bear in mind that the relative scaling of the two plots at this point is somewhat arbitrary. What is clear is that, for H loss from the $\beta - D$ propanal, the slow peak, which we assign to the hydroxyallyl isomer, is reduced by 50% relative to the undeuterated case, and this is true both for the *cis* and the *gauche* conformers. This observation supports the proposed dynamical behavior: after the D migration from C_β, the intermediate will be $CH_3CDCHDO^+$, and the chance of H loss from C_α would be half that of the corresponding intermediate $CH_3CHCH_2O^+$. The images of the D atom loss pathways are simpler: no outer ring is observed for either conformer. This is again consistent with the fact that the fast

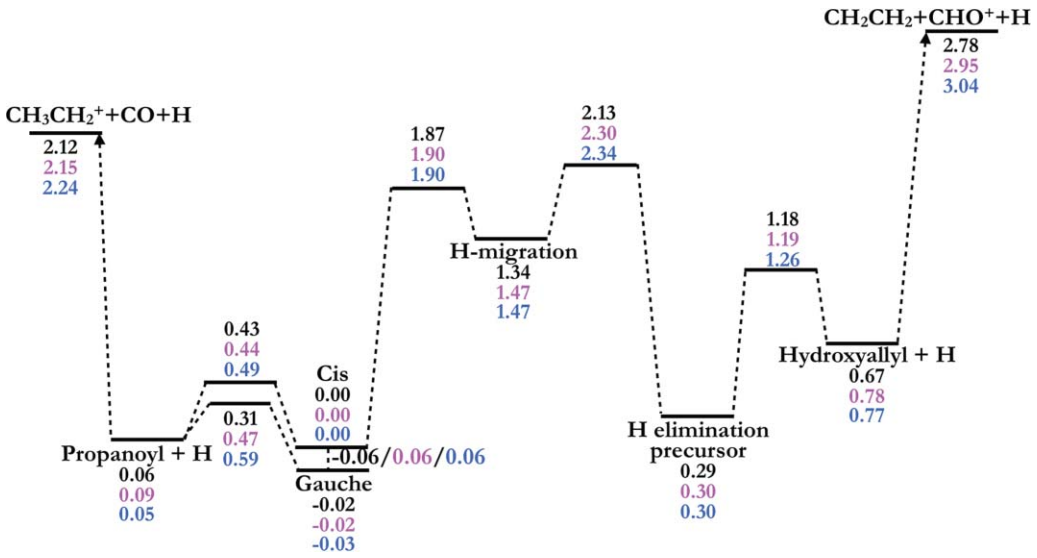

FIG. 12. Schematic pathways and energetics for normal ($CH_3CH_2CHO^+$, black), partially deuterated ($CH_3CD_2CHO^+$, purple), and fully deuterated ($CD_3CD_2CDO^+$, blue) propanal cation. Overall, the energetics does not change much for these isotopologues. However, the barrier heights from H migration structure to the slower channel increase faster than that from Hmigration structure back to propanal cation as we go from normal to fully deuterated propanalcation.

peak arises from loss of the aldehydic H atom to form the propanoyl cation. There is no D atom on the carbon, so D loss cannot give the propanoyl species. This also proves that the fast peak is direct elimination, without any isomerization process during the photodissociation. We note, as mentioned in the experimental section, the product of the deuterated propanal deuteration is a mixture, and the *gauche* transition is not fully spectroscopically selective. The *gauche* image, thus, shows both the peaks are mixed with the D loss from the $CH_3CD_2CHO^+$ and a sharp peak arising from H loss from the $CH_3CHDCHO$.

Similar excited state dynamics and ground state energetics calculations were performed for the partially deuterated propanal cation studied in the experiment as well as the fully deuterated propanal cation. No significant difference in the excited state mechanism was observed in the AIMS dynamics (but of course there could be subtle differences and much more extensive sampling of initial conditions would be required to quantify this). The energetics for all three isotopologues is compared in Fig. 12, and this is very similar to that for the undeuterated case shown in Fig. 8. The barrier from H-migration product to the H-elimination precursor increases somewhat more than that back to propanal. This will decrease the portion that goes to the slower channel. The branching ratios of the faster and slower channel for these three isotopologues (again computed by RRKM and kinetic modeling), starting from the H migration product, are listed in Table II. No significant isotope effects are observed. These results are consistent with the deuteration experiment (*vide supra*), which can be explained with little or no change in the basic mechanism.

A remaining question is the extent to which the conformer-specific dynamics reflect different energy content as opposed to true conformer specificity. We addressed this by measuring ion images for conformer-selected vibrationally excited propanal cation. Vibrationally excited propanal cation can be prepared through various (n, 3 s) REMPI transitions, and the mode selection purity can be verified from the respective photoelectron imaging experiments. Figure 13 illustrates the average ratio of the fast component with respect to the whole product as a function of the total available energy. For those transitions with broad photoelectron kinetic energy distribution, the kinetic energy release is averaged in the calculation of total available energy. The *cis* conformer with the lowest available energy has the lowest ratio of the fast product (direct H loss from the CHO group). For the ions with v_{15} (CCCO deformation) excitation, the relative yield of the fast product is more than that for the vibrationless *cis* cation. Among these transitions, four quanta excitation shows the largest yield of the fast product. For the v_{24} (CHO torsion) excitation, it is clear that one quantum of excitation increases the fast component and two quanta of this excitation significantly promote the enhancement. However, this trend is not observed for the v_{23} (CH_3 torsion) excitation. There is a region with the available energy above 3.58 eV : v_8 (formyl CH deformation), v_7/v_{11}(CH_2/scissor in-phase CCC stretch), V9 sym. (CH_3 deformation), v_{10} (CH_2 wag). The fast peak yield for one quantum in these modes is more than double

TABLE II. Branching ratios on the ground state starting from H migration product for three isotopologues of propanal cation: $CH_3CH_2CHO^+$, $CH_3CD_2CHO^+$, $CD_3CD_2CDO^+$. The partitioning between hydroxyallyl and propanoyl products does not exhibit a large isotope effect.

	$CH_3CH_2CHO^+$	$CH_3CD_2CHO^+$	$CD_3CD_2CDO^+$
Hydroxyallyl cation	22.0%	18.5%	18.3%
Propanoyl cation	78.0%	81.4%	81.6%

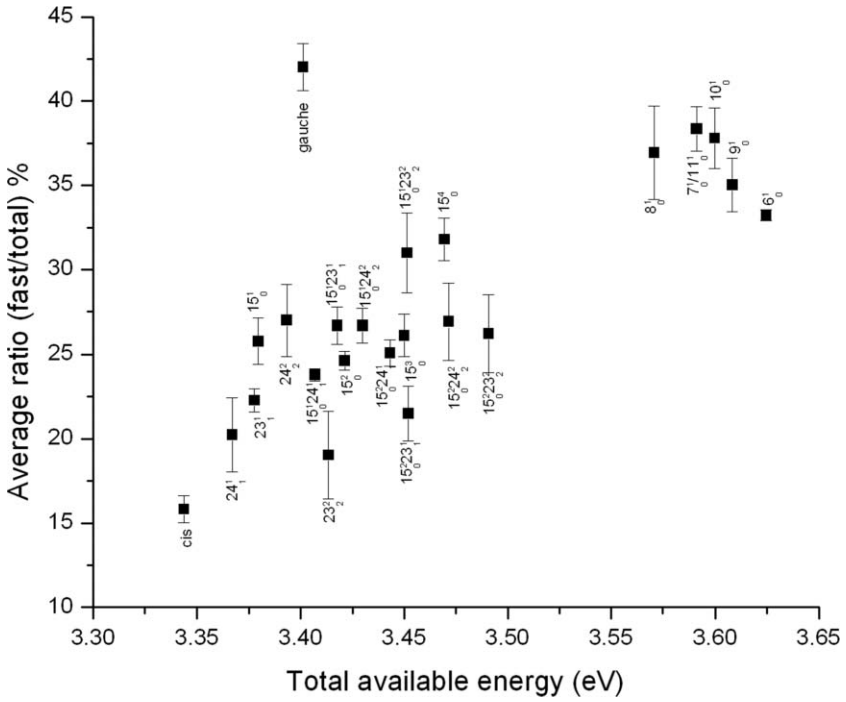

FIG. 13. The averaged ratio of fast and total product distribution as a function of total available energy of cations with specific vibrational state preparation.

that of the vibrationless *cis* conformer. However, the *gauche* conformer, with lower available energy, has the largest ratio of the fast peak, which means the conformation dependence is much larger than the energy effect alone. These results show a general trend revealing a greater yield of the fast peak with increasing energy. However, there are several transitions with almost the same available energy for photodissociation, for example: 23_2^2 and 15_0^1, $15_0^2 23_1^1$, 15_0^3, $15_0^1 23_2^2$, $15_0^2 24_2^2$ and 15_0^4. The product isomer yields for these excitations are significantly different, which indicates mode selectivity in this propanal cation system. This mode selectivity likely reflects similar issues related to those we have observed experimentally and characterized theoretically for the conformational dependence: Franck–Condon-mediated access to distinct regions of D_2/D_1 with coupling to different regions of the ground state. This mode selectivity is quite reproducible in the experiment and serves as a challenge for further modeling with the AIMS/RRKM treatment detailed here. Since the effect is rather subtle, this will require many more initial conditions and longer time scales in the AIMS simulations.

V. CONCLUSIONS

Ion imaging experiments reveal distinct photodissociation dynamics for propanal cations initially prepared in different molecular conformations and vibrational states. The kinetic energy release of the H elimination product is bimodal and the ratio of two products depends on the initial state preparation. Excited state dynamics simulations show the origin of the differing product branching ratios in the two conformers. Both conformers rapidly (within tens of fs) internally convert from the bright D_2 state to a dark D_1 state. However, they do so through *different* intersections, maintaining conformational memory. There are two pathways on the dark state available for both conformers. The *cis* conformer prefers the H migration pathway and tends to maintain this geometry as it returns to the electronic ground state. In contrast, the *gauche* conformer is more likely to undergo methyl-group migration, which regenerates propanal cation on return to the ground state. RRKM calculations on the ground state potential energy surface were carried out in order to determine the ultimate fate of the ground state species generated by photoexcitation of the *cis* or *gauche* conformers. These calculations show that the dissociation products depend on the ground state geometry. Thus, conformer specificity is observed in the products even though dissociation is statistical on the ground state. The conformer specificity of the dissociation products is a consequence of the ultrafast quenching to D_0 that retains conformational memory and populates distinct minima on D_0 according to the starting conformer. This is so even though the *cis* and *gauche* conformers are separated by only $\approx$400 cm^{-1} and the photon imparts $\approx$30 000 cm^{-1} of energy to the molecule. The difference between the yield of the slower channel for the *cis* and *gauche* conformers is predicted to be somewhat greater than a factor of 3. Although the total yield of the slower channel is rather small (13% and 4% for *cis* and *gauche*, respectively), the difference is clearly visible because most of the faster channel product is lost to secondary decomposition. This accentuates the signal in the ion image due to the slower channel which would otherwise be difficult to discern over the larger fast channel signal. In effect, facile secondary decomposition of propanoyl (fast channel) amplifies the apparent branching ratio. Experiments carried out on deuterated propanal are consistent with the proposed mechanistic picture. Further, experiments starting in different vibrational states show that there are reproducible mode-specific effects in addition to the conformer specificity. These same experiments also show that the conformer specific

dissociation cannot be explained on the basis of differences in the available energy. The observed mode specificity remains to be investigated theoretically, and future work will focus on this point.

ACKNOWLEDGMENTS

This work was supported in part under DOE Contract No. DE-AC02-7600515. The experimental work was supported by the NSF under award number CHE-0715300.

[1]L. Khriachtchev, E. Macuas, M. Pettersson, and M. Rasanen, J. Am. Chem. Soc. **124**, 10994 (2002).
[2]S. T. Park, S. K. Kim, and M. S. Kim, Nature (London) **415**, 306 (2002).
[3]T. A. A. Oliver, G. A. King, and M. N. R. Ashfold, J. Chem. Sci. **1**, 89 (2010).
[4]D. Shemesh and R. B. Gerber, J. Chem. Phys. **122**, 241104 (2005).
[5]M. H. Kim, L. Shen, H. Tao, T. J. Martinez, and A. G. Suits, Science **315**, 1561 (2007).
[6]S. L. Anderson, Adv. Chem. Phys. **82**, 177 (1992).
[7]M. N. R. Ashfold, N. H. Nahler, A. J. Orr-Ewing, O. P. J. Vieuxmaire, R. L. Toomes, T. N. Kitsopoulos, I. A. Garcia, D. A. Chestakov, S.-M. Wu, and D. H. Parker, Phys. Chem. Chem. Phys. **8**, 26 (2006).
[8]M. Ben-Nun and T. J. Martinez, Adv. Chem. Phys. **121**, 439 (2002).
[9]T. Baer and W. L. Hase, *Unimolecular Reaction Dynamics: Theory and Experiments*. (Oxford University Press, New York, 1996).
[10]T. Baer and P. M. Mayer, J. Am. Soc. Mass Spectrom. **8**, 103 (1997).
[11]C. C. Van De Sande and F. W. McLafferty, J. Am. Chem. Soc. **97**, 4617 (1975).
[12]C. E. Hudson and D. J. McAdoo, Org. Mass Spectrom. **17**, 366 (1982).
[13]C. E. Hudson and D.J. McAdoo, Org. Mass Spectrom. **19**, 1 (1984).
[14]J. C. Traeger, Org. Mass Spectrom. **20**, 223 (1985).
[15]W. J. Bouma, J. K. Macleod, and L. Radom, J. Am. Chem. Soc. **102**, 2246 (1980).
[16]G. Bouchoux, A. Luna, and J. Tortajada, Int. J. Mass Spectrom. Ion Process. **167/168**, 353 (1997).
[17]M. J. Polce and C. Wesdemiotis, J. Am. Soc. Mass Spectrom. **7**, 573 (1996).
[18]B. D. Leskiw, M. H. Kim, G. E. Hall, and A. G. Suits, Rev. Sci. Instrum. **76**, 104101 (2005).
[19]W. Li, S. D. Chambreau, S. A. Lahankar, and A. G. Suits, Rev. Sci. Instrum. **76**, 063106 (2005).
[20]E. J. Heller, J. Chem Phys. **62**, 1544 (1975).
[21]E. J. Heller, J. Chem Phys. **75**, 2923 (1981).
[22]M. Ben-Nun and T. J. Martinez, J. Chem. Phys. **108**, 7244 (1998).
[23]S. Yang, J. D. Coe, B. Kaduk, and T. J. Martinez, J. Chem Phys. **130**, 134113 (2009).
[24]A. L. Thompson, C. Punwong, and T. J. Martinez, Chem. Phys. **370**, 70 (2010).
[25]B. O. Roos, Acc. Chem. Res. **32**, 137 (1999).
[26]H.-J. Werner and P. J. Knowles, J. Chem Phys. **82**, 5053 (1985).
[27]P. J. Knowles and H.-J. Werner, Chem. Phys. Lett. **115**, 259 (1985).
[28]B. O. Roos, Acc. Chem. Res. **32**, 137 (1999).
[29]J. Finley, P. A. Malmqvist, B. O. Roos, and L. Serrano-Andres, Chem. Phys. Lett. **288**, 299 (1998).
[30]MOLPRO, a package of *ab initio* programs, designed by P. J. K. H.-J. Werner, R. Lindh, F. R. Manby, M. Schütz, and others, version 2006. see http://www.molpro.net
[31]B. G. Levine, J. D. Coe, A. M. Virshup, and T. J. Martinez, Chem. Phys. **347**, 3 (2008).
[32]G. Henkelman, B. P. Uberuaga, and H. Jonsson, J. Chem. Phys. **113**, 9901 (2000).
[33]M. H. Kim, L. Shen, and A. G. Suits, Phys. Chem. Chem. Phys. **8**, 2933 (2006).
[34]Essentially, we are appealing to valence bond arguments here in order to rationalize the possible structures.
[35]J. C. Ma and D. A. Dougherty, Chem. Rev. **97**, 1303 (1997).
[36]In a valence bond picture, one could also argue for resonance between the described CH3 + /CH2 = CHO structure and a CH2 = CHO + /CH3 structure stabilized by a three-center bond.
[37]C. E. Hudson, D. J. McAdoo, and J. C. Traeger, J. Am. Soc. Mass Spectrom. **13**, 1235 (2002).
[38]See supplementary material at http://dx.doi.org/10.1063/1.3540659 for coordinates and energies of minima and transition states, as well as reaction rates.
[39]J. R. Barker, Int. J. Chem. Kinet. **33**, 232 (2001).